

Nanoscale Ultrafine Zinc Metal Anodes for High Stability Aqueous Zinc Ion Batteries

Mingqiang Liu,[¶] Lu Yao,[¶] Yuchen Ji,[¶] Mingzheng Zhang, Yihang Gan, Yulu Cai, Hongyang Li, Wenguang Zhao, Yan Zhao, Zexin Zou, Runzhi Qin, Yuetao Wang, Lele Liu, Hao Liu, Kai Yang, Thomas S. Miller,* Feng Pan,* and Jinlong Yang*



Cite This: *Nano Lett.* 2023, 23, 541–549



Read Online

ACCESS |

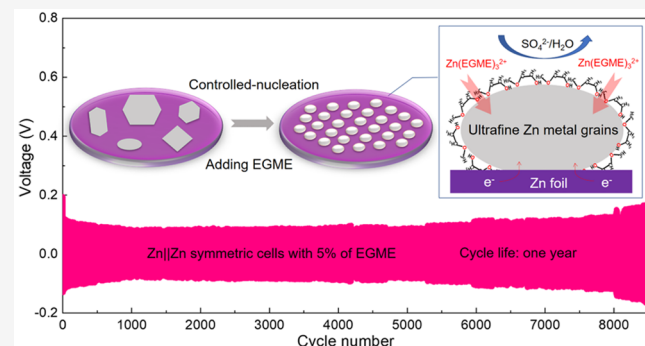
Metrics & More

Article Recommendations

Supporting Information

ABSTRACT: Aqueous Zn batteries (AZBs) are a promising energy storage technology, due to their high theoretical capacity, low redox potential, and safety. However, dendrite growth and parasitic reactions occurring at the surface of metallic Zn result in severe instability. Here we report a new method to achieve ultrafine Zn nanograin anodes by using ethylene glycol monomethyl ether (EGME) molecules to manipulate zinc nucleation and growth processes. It is demonstrated that EGME complexes with Zn^{2+} to moderately increase the driving force for nucleation, as well as adsorbs on the Zn surface to prevent H-corrosion and dendritic protuberances by refining the grains. As a result, the nanoscale anode delivers high Coulombic efficiency (ca. 99.5%), long-term cycle life (over 366 days and 8800 cycles), and outstanding compatibility with state-of-the-art cathodes (ZnVO and AC) in full cells. This work offers a new route for interfacial engineering in aqueous metal-ion batteries, with significant implications for the commercial future of AZBs.

KEYWORDS: Aqueous Zn batteries, zinc metal anode, ultrafine nanograins, dendrite growth, parasitic reactions



In order to address the energy crisis and environmental pollution, a major focus of human endeavor in recent decades has been the development of electrochemical energy storage and conversion systems to exploit renewable energy sources and achieve the goal of carbon neutrality.^{1–3} Aqueous zinc batteries (AZBs) are widely considered to be much safer and cheaper alternatives to lithium-ion batteries (LIBs), due to their high theoretical capacities (820 mAh g⁻¹) and the fact that they can operate in nonflammable and non-toxic aqueous electrolytes.^{1,4–8} However, the plating-stripping electrochemistry of zinc anodes in aqueous electrolytes has to date suffered from a low Coulombic efficiency (CE), caused by hydrogen evolution reaction (HER) corrosion side reactions associated with irreversible byproducts (Figure S1a).^{9,10} Large and disruptive hexagonal dendrites are easily formed in many AZBs, due to uneven deposition at the Zn metal surface, leading to capacity fading, consumption of electrolyte, and short circuits.^{11,12}

Many methods have been tried to obtain a homogeneous surface and improve the electrochemical performance of Zn metal anodes, such as modulating zinc electrodeposition behavior^{13,14,12,11,15,16}, surface modification,^{17–21} 3D structural anodes,^{22–25} novel separators,^{26,27} electrolyte additives (including salts,^{28–32} organic molecules^{2,33–38}), and more.³⁹ Electrolyte optimization has also been widely researched as

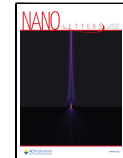
one of the most easy-to-implement and industrially relevant solutions, regulating the Zn^{2+} solvation sheath and introducing a stable solid electrolyte interphase, thereby inhibiting dendrite growth and the decomposition of H_2O .^{36,40–42}

Yet while, many of the above solutions have been proven to be effective in suppressing Zn dendrites growth or minimizing the HER and the formation of byproducts; few studies have focused on the issue of interfacial tension of electrolytes on metallic Zn surface, neglecting this crucial fundamental science. This is important as many of the problems associated with AZBs are exacerbated by the higher reactivity of metallic Zn in water-based electrolytes (−0.762 V vs standard hydrogen electrode (SHE)).^{28,36} According to the Nernst equation ($\Delta G_m = -nFE^0$),⁴³ the Gibbs free-energy ($\Delta G_m = -147 \text{ kJ mol}^{-1}$) of the reaction ($Zn + 2H^+ = Zn^{2+} + H_2$) is < 0 , meaning the spontaneity of Zn metal corrosion in zinc salt solutions⁴⁴ triggers a series of side reactions, including HER

Received: October 9, 2022

Revised: December 9, 2022

Published: January 3, 2023



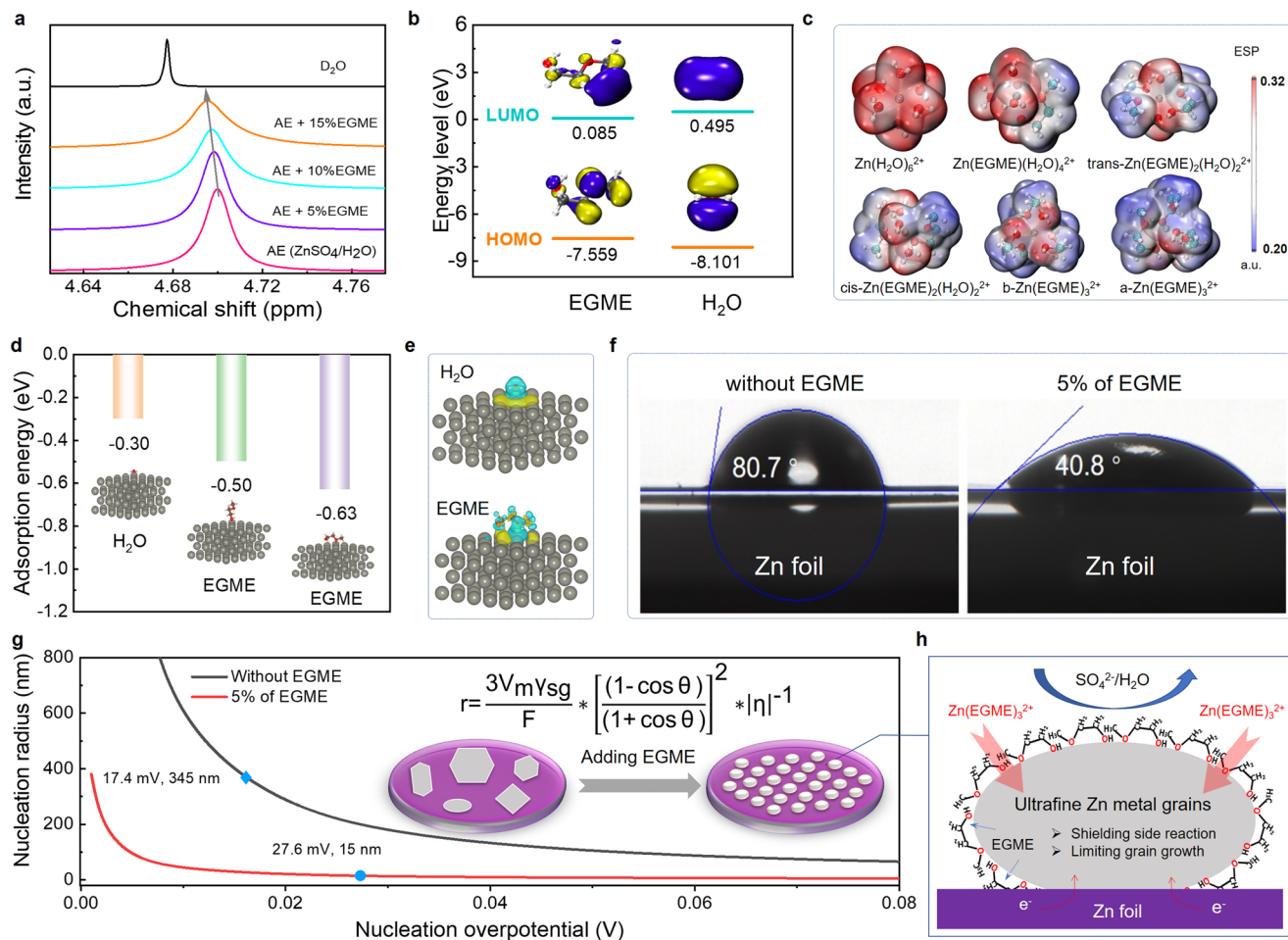


Figure 1. Theoretical studies. (a) ¹H NMR spectra of a 3 M ZnSO₄ aqueous electrolyte with different percentages of EGME added, from 0% to 15% in D₂O. (b) LUMO and HOMO isosurfaces of EGME (left) and water molecules (right), (isovalue = 0.02 au). (c) Electrostatic potential mapping of Zn²⁺ with H₂O and EGME molecule solvation structures. (d) Adsorption energy comparison of H₂O and EGME molecules on a Zn (002) crystal plane with different modes of adsorption. (e) Corresponding absorbed models for the different modes. The charge density difference between H₂O and EGME molecules adsorbed parallelly on Zn (002) crystal plane (yellow and light blue electron cloud clusters represent increase and decrease of electron density, respectively). (f) Wetting angles of ZnSO₄ electrolytes without/with EGME on Zn foil. (g) Graph of the relationship between critical zinc nuclei radius and zinc nucleation overpotential. Insets are zinc nuclei, illustrating the differences in size and density of deposited zinc nuclei under varying electrolyte interfacial tension. (h) Schematic diagram of zinc ion deposition process in electrolytes with EGEME.

and inert byproducts (eqs s1 and s2 in Figure S1a). Our prior work^{16,45} explored the use of a passivation layer to alter electrolyte surface tension, impede proton induced HER and protect the Zn metal from corrosion. But a simple and scalable method to controllably modulate electrolyte surface free energy and inhibit the activity of metallic zinc, thereby reducing side reactions and promoting uniform zinc deposition, is still required.

Herein, we propose a unique route to fabricate ultrafine grainy dendrite-free zinc metal anodes by decreasing the electrolyte surface tension and passivating the metallic Zn. Specifically, an organic molecule, ethylene glycol monomethyl ether (EGME), was introduced into a traditional ZnSO₄ electrolyte, which acts to both coordinate with Zn²⁺ ions to modulate the solvation structure and to chemisorb to the metallic Zn surface, thereby controllably increasing the driving force for zinc nucleation and growth, promoting uniform deposition and preventing side reactions (eq s3 in Figure S1b). It is demonstrated that the refined zinc anodes can realize a high average CE of 99.5% and promote ultralong-term cycling

stability over 8800 cycles (366 days). AC (activated carbon)||Zn full cells are also shown to display excellent cyclability, with negligible capacity fading over 10000 cycles, and larger pouch cells maintain near 100% retention over 1000 cycles, while full ZnVO_{1-x}Zn cells demonstrate that EGME is compatible with state-of-the-art ZIB cathodes. This simple method for controlling zinc anode interfacial structure and increasing AZB stability offers both a promising direction for understanding the mechanisms of zinc nucleation and growth in applied battery systems and a route for practically managing the anode instability issues that hold back the commercialization of AZBs and other energy storage systems.

THEORETICAL STUDIES

Theoretical calculations in scales ranging from atomistic-level quantum chemistry to molecule-level ab initio calculations were combined to investigate the deposition–dissolution process of zinc ions in AZBs. First, we investigated the effect of EGME molecules on the solvation structure of zinc ions. According to DFT calculations, the formation energy (Figure

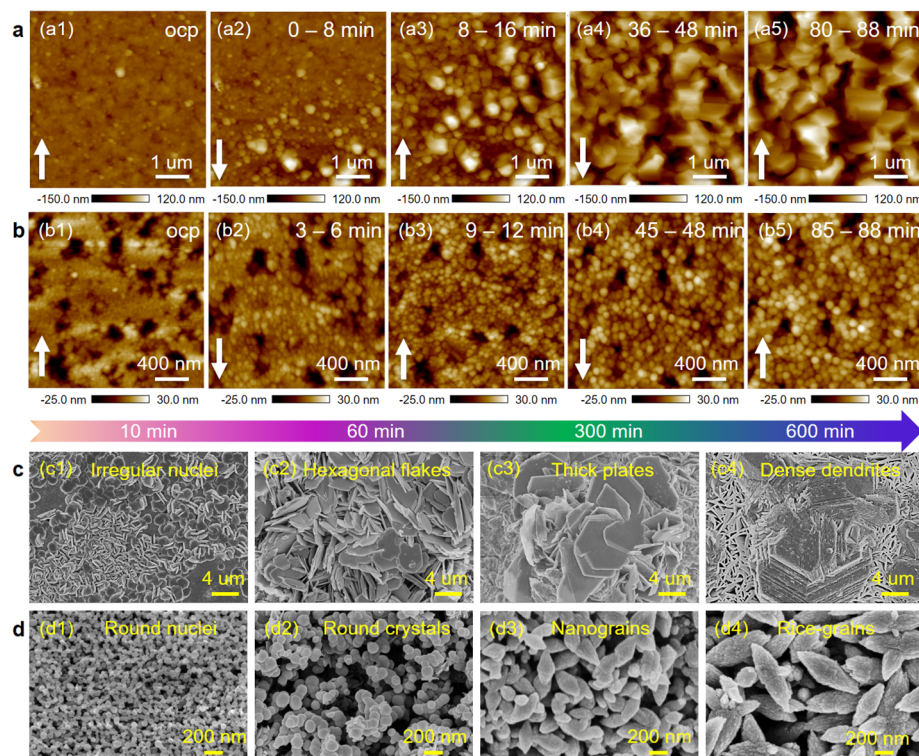


Figure 2. Structural evolution of the zinc anode. (a, b) In situ AFM images of zinc nucleation and growth process and (c, d) SEM morphology of Zn electrodeposits at different times (10, 60, 300, 600 min) (a, c) in ZnSO₄ electrolytes and (b, d) 5% of EGME added ZnSO₄ electrolytes.

S2) of Zn²⁺ coordinated with EGME is 0.48–1.52 eV lower than that of Zn²⁺ coordinated with H₂O molecules (−19.96 eV), meaning EGME can replace H₂O in the solvation shell to obtain a stable solvated structure. Experimental NMR measurements of EGME in ZnSO₄ electrolytes (Figure 1a and Figures S3 and S4) show peak movement to lower chemical shifts with the addition of EGME, which further demonstrate that EGME exhibits a strong tendency to complex with Zn²⁺ and displace water molecules from the typical solvation shell of [Zn(H₂O)₆]²⁺.

EGME molecules were also found to offer lower lowest unoccupied molecular orbital (LUMO) and higher highest occupied molecular orbital (HOMO) positions (Figure 1b) when compared to H₂O (0.085 eV vs 0.495 eV; −7.559 eV vs −8.101 eV), implying that EGME can more easily lose electrons. While comparison of the electrostatic potentials (ESP) (Figure 1c and Figure S5) further showed that replacing H₂O molecules in [Zn(H₂O)₆]²⁺ with EGME molecules is favorable.⁴⁶ This behavior is consistent with the altered electrochemical behavior observed from 2D diffusion in the traditional aqueous electrolyte to 3D diffusion in the EGME containing electrolyte (detailed analysis can be found in the SI and Figure S7a). Thus, it was demonstrated that the EGME molecule can facilitate the deposition–dissolution process of zinc ions in AZBs.

The interactions between a Zn foil and the different molecules was studied via Multiwfn software. The corresponding adsorption energy (Figure 1d) of H₂O and EGME via one or two O atoms on Zn (002) lattice plane were obtained to be −0.3, −0.5, and −0.63 eV, respectively, implying that strong binding via both EGME O sites to the Zn plane is preferential. Similar results were found when considering differences in charge density (Figure 1e). EGME was also found to adsorb

more strongly than H₂O at a number of Zn crystallographic planes (Figure S6), which may passivate the zinc metal to some extent and impact the nucleation–growth of zinc crystals.

Next, we explored the effect of EGME molecules on the zinc metal structure based on the nucleation–growth theory of electrodeposition.^{47–49} Voltage–time curves (Figure S7b) show two important characteristic overpotentials observed during galvanostatic Zn electrodeposition: (1) the nucleation overpotential (η_n), which is the magnitude of the voltage spike at the onset of Zn deposition, and (2) the plateau overpotential (η_p) present after nucleation occurs and Zn growth continues. The initial nucleation stage has a significant impact on the subsequent growth process as well as the structure and properties of the deposited products. Classical equations for homogeneous nucleation can be used to understand the dependence of the size of Zn nuclei on the electrodeposition overpotential and electrode and electrolyte properties. The nucleation radius (r) for forming a spherical nuclei is as follows:^{50,47}

$$r = \frac{3V_m\gamma_{sl}}{F} \times |\eta_n|^{-1} \quad (1)$$

Here r stands for the radius of zinc nuclei, V_m is the molar volume of zinc, F is Faraday's constant, γ_{sl} is the surface energy of the Zn-electrolyte interface, which can be calculated according to the combination of Young's equation⁵¹ and Fowkes equation⁵² and as follows:

$$\gamma_{sl} = \gamma_{sg} \left(\frac{1 - \cos \theta}{1 + \cos \theta} \right)^2 \quad (2)$$

Here γ_{sg} is the surface tension of the electrode and θ is the contact angle between the electrode and electrolyte, as shown

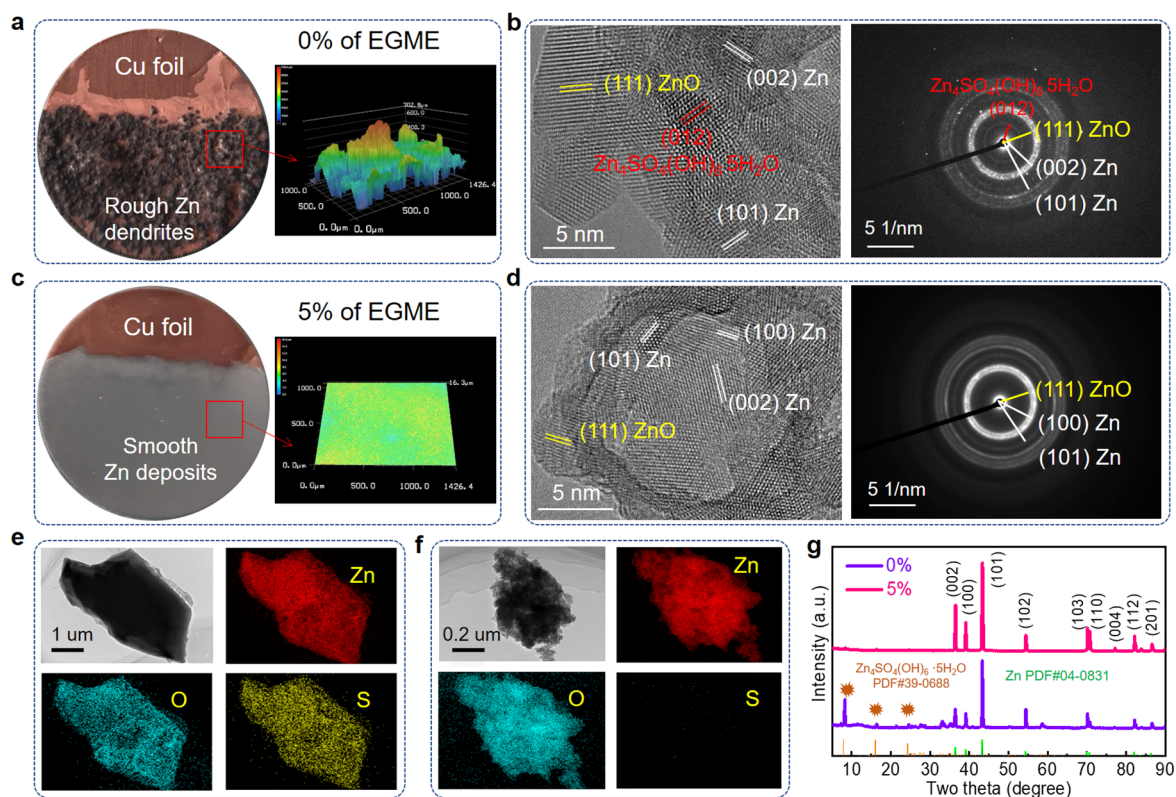


Figure 3. Structural characterization of zinc anodes. (a, b) Digital photos and corresponding 3D LCSM images of a Cu foil after electroplating, (c, d) HRTEM images and corresponding FFT patterns, (e, f) EDS maps of Zn, O, and S elements for zinc deposits at the Cu surface, and (g) XRD patterns of Zn foils after cycling ten times in (a, c, e, g) ZnSO₄ electrolytes and (b, d, f, g) 5% of EGME added ZnSO₄ electrolytes.

in Figure 1f. Since the electrode is a fixed invariant, the nucleation radius (r) is influenced mainly by η_n and the contact angle (θ) determined by the nature of the electrolyte, the derived equation is as follows:

$$r = \frac{3V_m\gamma_{sg}}{F} \times \left(\frac{1 - \cos \theta}{1 + \cos \theta} \right)^2 \times |\eta_n|^{-1} \quad (3)$$

It can be clearly observed that the size of Zn crystals can be effectively refined by directly manipulating the electrolyte to reduce the wetting angle of the electrolyte on the substrate and increased η_n . Interestingly, the contact angle of the electrolyte was greatly decreased to 40.8° after the addition of EGME, compared to 80.7° for the original ZnSO₄ (Figure 1f), indicating a greater surface free energy of the EGME solvent than water on zinc foils (Figure S18). The corresponding nucleus radius–overpotential curves (eq 3) at the two wetting angles are presented in Figure 1g, where it can be seen that all of the zinc nuclei in the EGME-added electrolyte had radii that were consistently below those in the ZnSO₄ electrolyte. Typically, an overpotential of 27.6 mV at a current density of 0.5 mA cm⁻² in the traditional electrolyte corresponds to a nucleation radius of 345 nm, whereas an overpotential of 17.4 mV in an EGME-added electrolyte at the same current density corresponds to a nucleation radius of 15 nm, demonstrating that EGME molecules can achieve grain refinement through controlled nucleation. Therefore, this demonstrates that the EGME molecules with their optimal dioxygen functional groups replace H₂O molecules in complex with Zn ions to increase the driving force for nucleation, as well as adsorbing on the metallic Zn surface and act as a passivation layer to prevent corrosion, regulating Zn deposition at kinetically

favored sites, refining grains, promoting even growth and blocking dendritic protuberances (Figure 1h).

STRUCTURAL EVOLUTION OF ZINC ANODES

The morphology of zinc nuclei and subsequent crystal growth under the regulation of EGME was uncovered by operando electrochemical atomic force microscopy (EC-AFM, set up shown in Figure S8), combined with ex situ scanning electron microscopy (SEM) and transmission electron microscopy (TEM). All operando EC-AFM images of galvanostatic Zn electrodeposition on Cu foil between 0 and 88 min at 0.1 mA cm⁻² are shown in Figure S9 and Figure S10, with select zoomed sections highlighted in Figure 2, parts a and b. In original electrolyte small irregular-shaped zinc crystals can be seen to be produced at the early stages of electrodeposition and some of them gradually grow into large quasi-hexagonal zinc grains with edges and corners (Figure 2a2). After 88 min, the size of the zinc protrusions has reached 1–2 μm (Figure 2a5). In contrast, with the addition of EGME, the early zinc crystals are much smaller and more regular round particles (Figure 2b2). Thereafter, zinc nanograins grow slightly into spherical pellets that are tightly packed together, eventually forming a homogeneous surface with zinc nanoparticles of ~100 nm (Figure 2b5). 3D AFM images (Figure S11) and corresponding surface roughness measurements (Figure S12) highlight the significant difference in Zn deposition morphology. The quantified surface roughness value (Ra) of the Zn on Cu in pure ZnSO₄ increases dramatically from 9.4 at open circuit potential (OCP) to 20.4, 33.5, 39.5, and 47.5 from 0 to 8, 8 to 16, 36 to 48 and 80 to 88 min respectively, whereas the

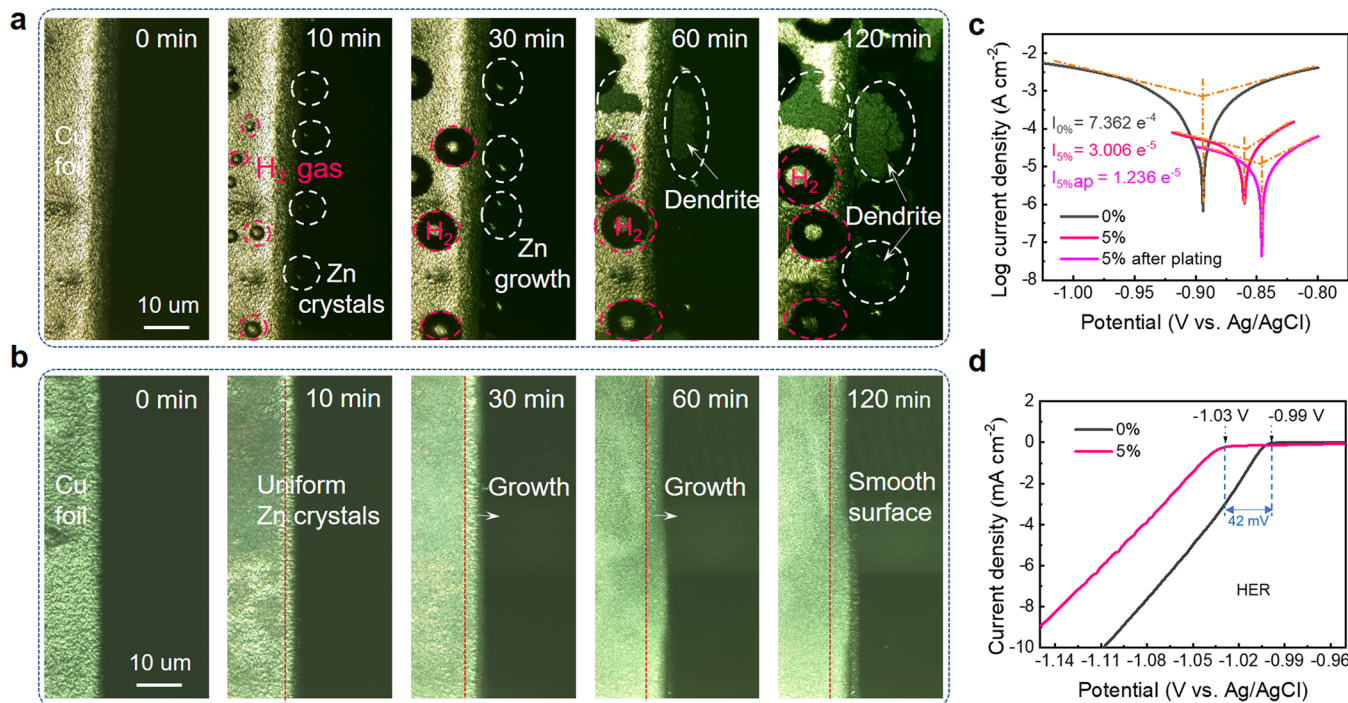


Figure 4. Zinc Plating/Stripping Behaviors. (a, b) In situ optical LCSM images of Zn plating behavior on Cu foils at 10 mA cm^{-2} , (c) Tafel plots of a bare Zn foil before plating and after plating 3 h, and (d) HER plots of a bare Zn foil with a three-electrode system in (a, c, d) ZnSO_4 electrolytes and (b, c, d) 5% of EGME added ZnSO_4 electrolytes.

sample in the EGME-modified electrolyte remained almost unchanged at $\sim 8.0 \text{ Ra}$ (Figure S13).

SEM images further show the differing microstructure of zinc electrodeposits between 10 and 600 min (Figure 2, parts c and d) (detailed analysis can be found in Figures S14–S17). The average size of Zn flakes after 300 min of deposition was $7.0 \mu\text{m}$ (Figure S16a–c), a size that would certainly cause damage within an operational AZBs. However, by regulating deposition using EGME, the zinc crystals grew into prolate spheroid (i.e., rice-shaped) nanopellets of $\sim 250 \text{ nm}$ (Figure S16d–f), and then self-assembled into bigger nanocrystals of $\sim 400 \text{ nm}$ after 600 min (Figure 2d4).

Macroscale images of zinc electrodeposits on copper foil surfaces in electrolytes without/with EGME are shown in Figure 3, highlighting a stark morphological contrast. It can be clearly observed from Figure 3a that the surface of the Cu foil after plating in ZnSO_4 electrolytes is black-brown and very rough. 3D laser confocal scanning microscope (LCSM) shows a surface roughness of over $700 \mu\text{m}$. Interestingly, TEM imaging and electron diffraction data (Figure 3b) confirm the presence of $\text{Zn}_4\text{SO}_4(\text{OH})_6 \cdot 5\text{H}_2\text{O}$ byproducts in the pure ZnSO_4 cycled electrode, which has been linked to poor cycling performance and dendrite proliferation,⁵³ alongside ZnO (suggesting oxidization after air exposure). In contrast, with the addition of EGME, the macroscale surface of the Zn coated Cu foil is extremely smooth with a zinc–metallic luster, consistent with the micro/nanoscale data (Figure 3c). The LCSM measured surface roughness was dramatically reduced to just $16.3 \mu\text{m}$, over 43 times lower, highlighting grain refining effect of EGME molecules. Meanwhile, no detrimental $\text{Zn}_4\text{SO}_4(\text{OH})_6 \cdot 5\text{H}_2\text{O}$ could be found from the surface of a single spherical particle under TEM (Figure 3d), only contributions from ZnO . In addition, energy dispersive X-ray spectroscopy (EDS) mapping from both SEM (Figure S18a)

and Table S1) and TEM (Figure 3e and Table S2) shows that the electrode cycled in pure ZnSO_4 presents a significant S contribution (6.5 wt % TEM-EDS, 4.9 wt % SEM-EDS), implying large amounts of SO_4^{2-} derived species have been formed during electrodeposition. However, little S was detected at the surface of the electrode cycled in EGME (0.08 wt % TEM-EDS, Figure 3f and Table S2, and 0.09 wt % SEM-EDS, Figure S18 and Table S1). The morphology of Zn foil electrodes after stripping for 600 min shows similar behavior (Figure S19), implying a strong contrast in heterogeneous and homogeneous reactive sites. X-ray diffraction patterns (XRD) and X-ray photoelectron spectroscopy (XPS) (Figure 3g and Figures S20–S22) of the cycled Zn anode with EGME further demonstrated that minimal amounts of byproducts were produced, showing that EGME has a significant ability to minimize parasitic reactions during cycling (detailed analysis can be found in the Supporting Information).

ZINC PLATING/STRIPPING BEHAVIORS

In order to explore the relationship between the morphology of the Zn deposits and the electrochemical behavior, in situ optical LCSM was utilized to monitor the structural evolution of Cu foils during the Zn plating process. Snapshots of a cross section of Cu foil at different stages of deposition, with/without EGME, are shown in Figure 4a and b. At OCP, the surface of Cu foil is very smooth in both cases, but after a constant current of 10 mA cm^{-2} was applied, uneven zinc crystals appeared on the Cu surface in the pure electrolyte, accompanied by a large number of H_2 bubbles. Subsequently, after 60 mins of electrodeposition, zinc ions can be seen to deposit preferentially around the as-formed zinc crystal nuclei to form large moss-like protuberances with thicknesses up to $\sim 15 \mu\text{m}$. On the contrary, in the electrolyte with EGME, zinc

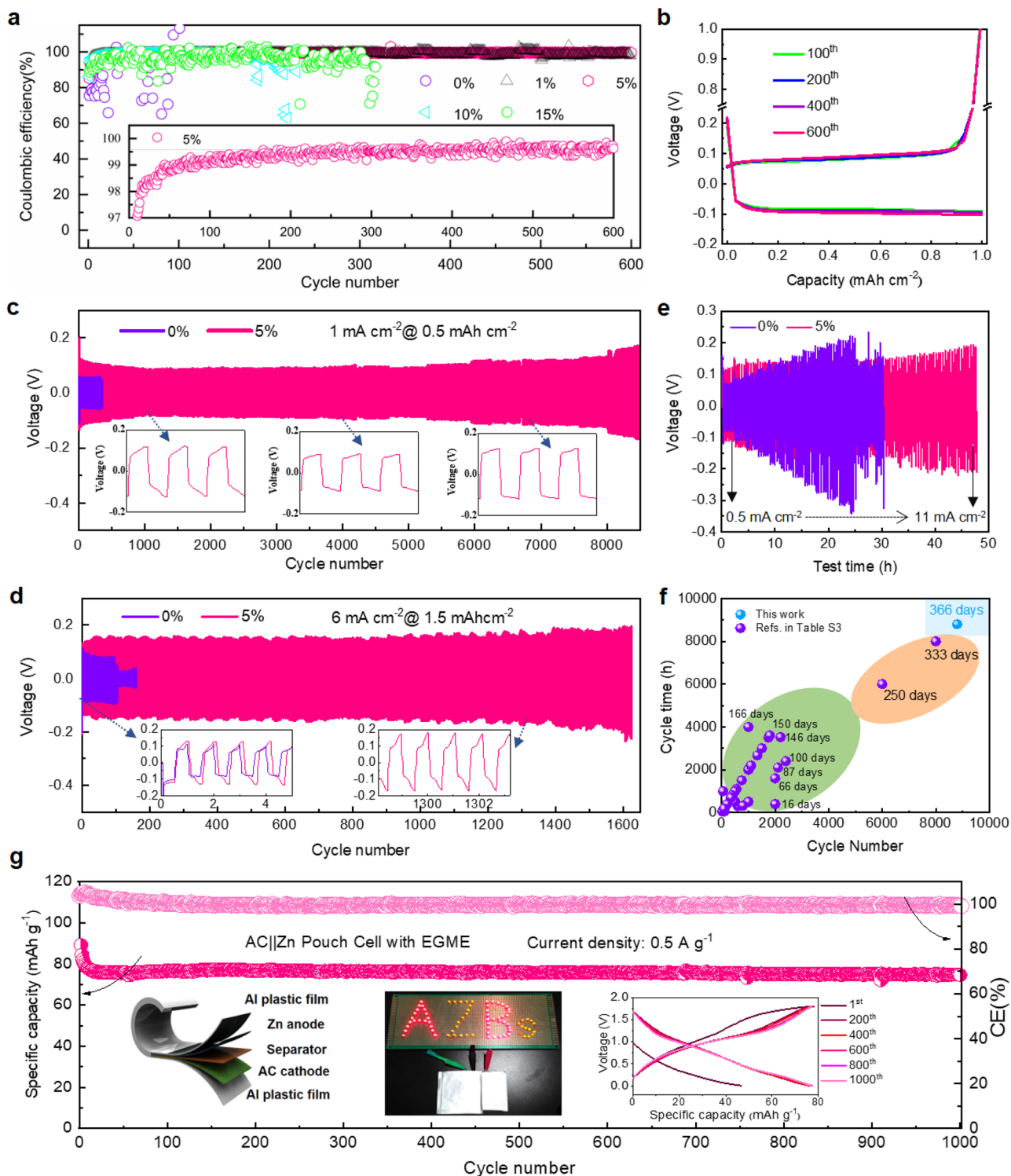


Figure 5. Electrochemical performance of half and full cells. (a) Coulombic efficiency of Cu||Zn cells in electrolytes with different percentages of EGME, from 0% to 15% at a current density of 2 mA cm^{-2} , 1 mAh cm^{-2} . (b) Polarization curves of Cu||Zn cells in electrolytes with 5% EGME additive at the 100th, 200th, 400th, and 600th cycles, respectively. Long-term cycling performance at (c) 1 mA cm^{-2} , 0.5 mAh cm^{-2} and at (d) 6 mA cm^{-2} , 1.5 mAh cm^{-2} for Zn||Zn symmetric cells without/with 5% of EGME. Insets are the corresponding high-resolution voltage profiles. (e) Rate performance from 0.5 to 11 mA cm^{-2} for Zn||Zn symmetric cells without/with 5% of EGME. (f) Comparison of the cyclability of Zn||Zn symmetric cells previously reported with various additives and those from this work. (g) Long-term cycling performance for AC||Zn full pouch cell with 5% of EGME additive at a current density of 0.5 A g^{-1} . Insets are a digital picture of two pouch cells connected in series lighting a LED board, a schematic diagram of pouch cell and the corresponding galvanostatic charge/discharge curves.

ions deposited evenly on the Cu foil without any site specific accumulation, eventually forming a homogeneous layer. No H₂ bubbling or zinc dendritic protrusions could be observed on

the surface even after long-term electrodeposition. Hindering HER is extremely beneficial for AZBs, as this is a significant mode of cell degradation and electrolyte loss, making

commercialization easier as cells will not have to be designed to counter the effects of gassing. When the above deposited Cu foils were observed under LCSM and SEM ([Figure S23](#)), areas where Zn has not deposited could easily be observed for the 0% sample, indicating uneven zinc deposition. For the 5% sample, no unreacted regions could be seen across millimeter scale regions. EDS tests ([Figure S24](#), top view, and [Figure S25](#), cross section) further affirm the uniform deposition.

The positive effect of EGME on the corrosion resistance of Zn foils was verified by Tafel and HER onset potential tests in [Figure 4c](#) and d (a detailed analysis can be found in the [Supporting Information](#)). These results imply that EGME molecules tend to adsorb on the zinc surface and form a protective layer, much like the solid–electrolyte interface in LIBs. During electroplating, this layer forms via strong chemisorption to inhibit the spontaneous corrosion and undesirable side-reactions.

ELECTROCHEMICAL PERFORMANCE

We evaluated the effect of zinc grain refinement by EGME molecules on battery performance through reversible Zn plating/stripping measurements. First, the zinc CE was measured using Zn||Cu coin cells, as shown in [Figure 5a](#), [Figure S26](#), and [Figure S27](#). The CE of Zn||Cu cells with the traditional electrolyte fluctuated greatly, gradually decreasing to below 60% after \sim 50 cycles at 2 mA cm^{-2} , 1 mAh cm^{-2} , likely due to zinc protrusion, the growth of byproducts, or the HER. In contrast, the zinc CE gradually increased and became more stable with the regulation of EGME. With 5% EGME first cycle Zn plating/stripping efficiency was 85.2%, exceeded 97.5% after 10 cycles, and reached an average CE of 99.5% from the 50th to 600th cycle. The corresponding polarization curves are also highly consistent from the 50th to 600th cycles ([Figure 5b](#)), further demonstrating the significantly stability. Zn||Cu coin cells with 5% EGME electrolytes also achieved excellent zinc CE at 1 mA cm^{-2} , 1 mAh cm^{-2} , with an average CE of 99.5% for 400 cycles ([Figure S26a](#)), and at 6 mA cm^{-2} , 0.5 mAh cm^{-2} , with an average CE of 98.5% over 1100 cycles ([Figure S26b](#)).

The cycling stability of metallic Zn electrodes was also investigated in Zn||Zn symmetric cells ([Figure 5c](#) and d), showing the 5% EGME additive cells could achieve a cycle life of over 8800 cycles (366 days) at 1 mA cm^{-2} , 0.5 mAh cm^{-2} , compared to \sim 200 cycles with the traditional ZnSO₄ electrolyte, an extremely significant improvement. Even at higher current densities, the Zn symmetric cells exhibited excellent performance: over 1600 cycles at 6 mA cm^{-2} , 1.5 mAh cm^{-2} ([Figure 5d](#)), and over 200 cycles at 12 mA cm^{-2} , 3 mAh cm^{-2} ([Figure S28](#)). The rate performance of the symmetric coin cells with the additive was also greatly improved ([Figure 5e](#); detailed analysis can be found in [Figures S29](#) and [S30](#) along with a relevant discussion). The excellent cycling performance of these Zn||Zn symmetric cells in this study compares very favorably with previous reports which report the use of electrolyte additives, exceeding previously reported cycle life and rate performance ([Figure 5f](#) and [Table S3](#)).

Finally, we employed AC or ZnVO ($\text{Zn}_{0.25}\text{V}_2\text{O}_5$) cathodes and a Zn metal anode to assemble commercially viable full cells to evaluate the impact of electrolytes with EGME as an additive (detailed electrochemical information can be found in [Figures S31–S34](#)). When tested in cells with a traditional faradaic AZB cathode, namely ZnVO||Zn coin cells ([Figure](#)

S35a), the EGME additive enables significant cell stabilization. AC cathodes then were studied to avoid complications due to cathode-specific degradation. The full coin cells with EGME offer an ultralong cycle lifespan of over 10000 cycles, with near 100% CE. Importantly, this significant performance enhancement is sustained in practical AC||Zn pouch cells ([Figure 5g](#)), where EGME promoted extremely high stability (sustaining near 100% CE after 1000 cycles). Hence, this data suggests that EGME has anode stabilization properties that can be applied widely across ZIB chemistries.

In summary, we report a simple and easily scalable method to fundamentally solve the problem of Zn anode instability via an organic molecule, EGME, which is shown to moderately decrease the surface tension for aqueous electrolytes to form ultrafine nanograins, significantly enhancing cycling reversibility and inhibiting dendrites and hydrogen evolution. Combined *in situ*/*operando* experiments and theoretical calculations reveal that EGME both complexes with Zn ions in solution and forms an anode passivation layer, hindering cell degradation. Importantly, through the use of this scalable low percentage additive, a compact, uniform and highly reversible surface is maintained at Zn anodes for long (\sim 10 000 cycle) lifetimes in full cells at high CE. This methodology and mechanistic understanding therefore offers a promising and simple to implement route for the commercial application of highly reversible, highly safe, and high energy density aqueous batteries at scale and, more widely, offers an approach by which the application of other multivalent battery chemistries could be realized.

ASSOCIATED CONTENT

Supporting Information

The Supporting Information is available free of charge at <https://pubs.acs.org/doi/10.1021/acs.nanolett.2c03919>.

Details about materials synthesis and characterizations, battery assembly and electrochemical measurement, and discussion sections ([PDF](#))

AUTHOR INFORMATION

Corresponding Authors

Thomas S. Miller – *Electrochemical Innovation Lab, Department of Chemical Engineering, University College London, London WC1E 7JE, U.K.*;  orcid.org/0000-0002-2224-5768; Email: t.miller@ucl.ac.uk

Feng Pan – *School of Advanced Materials, Peking University Shenzhen Graduate School, Shenzhen 518055, P. R. China*;  orcid.org/0000-0002-8216-1339; Email: panfeng@pkusz.edu.cn

Jinlong Yang – *Guangdong Research Center for Interfacial Engineering of Functional Materials, College of Materials Science and Engineering, Shenzhen University, Shenzhen 518060, P. R. China*;  orcid.org/0000-0001-6065-7272; Email: yangjl18@szu.edu.cn

Authors

Mingqiang Liu – *Guangdong Research Center for Interfacial Engineering of Functional Materials, College of Materials Science and Engineering, Shenzhen University, Shenzhen 518060, P. R. China*; *School of Advanced Materials, Peking University Shenzhen Graduate School, Shenzhen 518055, P. R. China*; *Electrochemical Innovation Lab, Department of*

- Chemical Engineering, University College London, London WC1E 7JE, U.K.
- Lu Yao** — School of Advanced Materials, Peking University Shenzhen Graduate School, Shenzhen 518055, P. R. China
- Yuchen Ji** — School of Advanced Materials, Peking University Shenzhen Graduate School, Shenzhen 518055, P. R. China
- Mingzheng Zhang** — School of Advanced Materials, Peking University Shenzhen Graduate School, Shenzhen 518055, P. R. China
- Yihang Gan** — Guangdong Research Center for Interfacial Engineering of Functional Materials, College of Materials Science and Engineering, Shenzhen University, Shenzhen 518060, P. R. China
- Yulu Cai** — School of Advanced Materials, Peking University Shenzhen Graduate School, Shenzhen 518055, P. R. China
- Hongyang Li** — School of Advanced Materials, Peking University Shenzhen Graduate School, Shenzhen 518055, P. R. China
- Wenguang Zhao** — School of Advanced Materials, Peking University Shenzhen Graduate School, Shenzhen 518055, P. R. China
- Yan Zhao** — Department of Mechanical Engineering, Imperial College London, London SW7 2AZ, U.K.
- Zexin Zou** — Guangdong Research Center for Interfacial Engineering of Functional Materials, College of Materials Science and Engineering, Shenzhen University, Shenzhen 518060, P. R. China
- Runzhi Qin** — School of Advanced Materials, Peking University Shenzhen Graduate School, Shenzhen 518055, P. R. China
- Yuetao Wang** — School of Advanced Materials, Peking University Shenzhen Graduate School, Shenzhen 518055, P. R. China
- Lele Liu** — School of Advanced Materials, Peking University Shenzhen Graduate School, Shenzhen 518055, P. R. China
- Hao Liu** — School of Chemical Engineering and Advanced Materials, The University of Adelaide, North Terrace, South Australia 5005, Australia
- Kai Yang** — Department of Electrical and Electronic Engineering, University of Surrey, Guildford, Surrey GU2 7XH, U.K.

Complete contact information is available at:
<https://pubs.acs.org/10.1021/acs.nanolett.2c03919>

Author Contributions

✉ M.L., L.Y., and Y.J. contributed equally to this work.

Notes

The authors declare no competing financial interest.

ACKNOWLEDGMENTS

This work was financially supported by a University College London Dean's Prize and China Scholarships Council funding, the National Natural Science Foundation of China (52172217), the Natural Science Foundation of Guangdong Province (2021A1515010144), and the Shenzhen Science and Technology Program (JCYJ20210324120400002). We also appreciate the U.K. Faraday Institution (EP/S003053/1) for support via the LiSTAR Project (FIRG014). We are thankful for the support from the Test Center of the SAM-PKUSZ for Micro and Nanoscale Research and Fabrication, and the advanced computing resources from the Supercomputing Center of the SAM-PKUSZ.

REFERENCES

- (1) Han, D.; et al. A non-flammable hydroxyl organic electrolyte for sustainable zinc batteries. *Nat. Sustain.* **2022**, *5*, 205–213.
- (2) Hao, J.; et al. Boosting Zinc Electrode Reversibility in Aqueous Electrolytes by Using Low-Cost Antisolvents. *Angew. Chem. Int. Ed.* **2021**, *60*, 7366–7375.
- (3) Jia, X.; Liu, C.; Neale, Z. G.; Yang, J.; Cao, G. Active Materials for Aqueous Zinc Ion Batteries: Synthesis, Crystal Structure, Morphology, and Electrochemistry. *Chem. Rev.* **2020**, *120*, 7795–7866.
- (4) Ma, L.; et al. Realizing high zinc reversibility in rechargeable batteries. *Nat. Energy* **2020**, *5*, 743–749.
- (5) Tang, B.; Shan, L.; Liang, S.; Zhou, J. Issues and opportunities facing aqueous zinc-ion batteries. *Energy Environ. Sci.* **2019**, *12*, 3288–3304.
- (6) Blanc, L. E.; Kundu, D.; Nazar, L. F. Scientific Challenges for the Implementation of Zn-Ion Batteries. *Joule* **2020**, *4*, 771–799.
- (7) Zhang, S.; et al. Polyiodide Confinement by Starch Enables Shuttle-Free Zn–Iodine Batteries. *Adv. Mater.* **2022**, *34*, 2201716.
- (8) Liu, M.; et al. Tuning phase evolution of β -MnO₂ during microwave hydrothermal synthesis for high-performance aqueous Zn ion battery. *Nano Energy* **2019**, *64*, 103942.
- (9) Chao, D.; et al. Roadmap for advanced aqueous batteries: From design of materials to applications. *Sci. Adv.* **2020**, *6*, eaba4098.
- (10) Hao, J.; et al. An In-Depth Study of Zn Metal Surface Chemistry for Advanced Aqueous Zn-Ion Batteries. *Adv. Mater.* **2020**, *32*, 2003021.
- (11) Yang, Q.; et al. Hydrogen-Substituted Graphdiyne Ion Tunnels Directing Concentration Redistribution for Commercial-Grade Dendrite-Free Zinc Anodes. *Adv. Mater.* **2020**, *32*, 2001755.
- (12) Yuksel, R.; Buyukcakir, O.; Seong, W. K.; Ruoff, R. S. Metal-Organic Framework Integrated Anodes for Aqueous Zinc-Ion Batteries. *Adv. Energy Mater.* **2020**, *10*, 1904215.
- (13) Zheng, J.; et al. Spontaneous and field-induced crystallographic reorientation of metal electrodeposits at battery anodes. *Sci. Adv.* **2020**, *6*, eabb1122.
- (14) Zheng, J.; et al. Regulating electrodeposition morphology in high-capacity aluminium and zinc battery anodes using interfacial metal–substrate bonding. *Nat. Energy* **2021**, *6*, 398–406.
- (15) Kang, L.; et al. Nanoporous CaCO₃ Coatings Enabled Uniform Zn Stripping/Plating for Long-Life Zinc Rechargeable Aqueous Batteries. *Adv. Energy Mater.* **2018**, *8*, 1801090.
- (16) Liu, M.; et al. Artificial Solid-Electrolyte Interface Facilitating Dendrite-Free Zinc Metal Anodes via Nanowetting Effect. *ACS Appl. Mater. Interfaces* **2019**, *11*, 32046–32051.
- (17) Zhang, Q.; et al. Revealing the role of crystal orientation of protective layers for stable zinc anode. *Nat. Commun.* **2020**, *11*, 3961.
- (18) Zhi, J.; Li, S.; Han, M.; Chen, P. Biomolecule-guided cation regulation for dendrite-free metal anodes. *Sci. Adv.* **2020**, *6*, eabb1342.
- (19) Xie, X.; et al. Manipulating the ion-transfer kinetics and interface stability for high-performance zinc metal anodes. *Energy Environ. Sci.* **2020**, *13*, 503.
- (20) Zheng, J.; et al. Reversible epitaxial electrodeposition of metals in battery anodes. *Science* **2019**, *366*, 645–648.
- (21) Zhang, Y.; Howe, J. D.; Ben-yoseph, S.; Wu, Y.; Liu, N. Unveiling the Origin of Alloy-Seeded and Nondendritic Growth of Zn for Rechargeable Aqueous Zn Batteries. *ACS Energy Lett.* **2021**, *6*, 404–412.
- (22) Parker, J. F.; et al. Rechargeable nickel–3D zinc batteries: An energy-dense, safer alternative to lithium-ion. *Science* **2017**, *356*, 415–418.
- (23) Zeng, Y.; et al. Dendrite-Free Zinc Deposition Induced by Multifunctional CNT Frameworks for Stable Flexible Zn-Ion Batteries. *Adv. Mater.* **2019**, *31*, 1903675.
- (24) Wang, Z.; et al. A Metal-Organic Framework Host for Highly Reversible Dendrite-free Zinc Metal Anodes. *Joule* **2019**, *3*, 1289–1300.

- (25) Zhang, Q.; Luan, J.; Tang, Y.; Ji, X.; Wang, H. Interfacial Design of Dendrite-Free Zinc Anodes for Aqueous Zinc-Ion Batteries *Angewandte. Angew. Chem. Int. Ed.* **2020**, *59*, 13180–13191.
- (26) Zhang, X.; et al. Ultra-long-life and highly reversible Zn metal anodes enabled by a desolvation and deionization interface layer. *Energy Environ. Sci.* **2021**, *14*, 3120.
- (27) Cui, Y.; et al. An Interface-Bridged Organic–Inorganic Layer that Suppresses Dendrite Formation and Side Reactions for Ultra-Long-Life Aqueous Zinc Metal Anodes. *Angew. Chem. Int. Ed.* **2020**, *59*, 16594–16601.
- (28) Wang, F.; et al. Highly reversible zinc metal anode for aqueous batteries. *Nat. Mater.* **2018**, *17*, 543–550.
- (29) Zhang, Q.; Ma, Y.; Lu, Y.; Li, L.; Wan, F.; Zhang, K.; Chen, J.; et al. Modulating electrolyte structure for ultralow temperature aqueous zinc batteries. *Nat. Commun.* **2020**, *11*, 4463.
- (30) Wu, X.; Xu, Y.; Zhang, C.; Leonard, D. P.; Markir, A.; Lu, J.; Ji, X. Reverse Dual-Ion Battery via a ZnCl₂ Water-in-Salt Electrolyte. *J. Am. Chem. Soc.* **2019**, *141*, 6338–6344.
- (31) Cai, S.; et al. Water–Salt Oligomers Enable Supersoluble Electrolytes for High-Performance Aqueous Batteries. *Adv. Mater.* **2021**, *33*, 2007470.
- (32) Guo, X.; et al. Alleviation of Dendrite Formation on Zinc Anodes via Electrolyte Additives. *ACS Energy Lett.* **2021**, *6*, 395–403.
- (33) Sun, P.; et al. Simultaneous Regulation on Solvation Shell and Electrode Interface for Dendrite-Free Zn Ion Batteries Achieved by a Low-Cost Glucose Additive Research Articles. *Angew. Chem. Int. Ed.* **2021**, *60*, 18247–18255.
- (34) Chang, N.; et al. An aqueous hybrid electrolyte for low-temperature zinc-based energy storage devices. *Energy Environ. Sci.* **2020**, *13*, 3527.
- (35) Naveed, A.; et al. A Highly Reversible Zn Anode with Intrinsically Safe Organic Electrolyte for Long-Cycle-Life Batteries. *Adv. Mater.* **2019**, *31*, 1900668.
- (36) Cao, L.; et al. Solvation Structure Design for Aqueous Zn Metal Batteries. *J. Am. Chem. Soc.* **2020**, *142*, 21404–21409.
- (37) Zhao, F.; et al. Trace amounts of fluorinated surfactant additives enable high performance zinc-ion batteries. *Energy Storage Mater.* **2022**, *53*, 638–645.
- (38) Dong, H.; Hu, X.; He, G. A shear-thickening colloidal electrolyte for aqueous zinc-ion batteries with resistance on impact. *Nanoscale* **2022**, *14*, 14544–14551.
- (39) Yuan, L.; Hao, J.; Kao, C.; Wu, C.; Liu, H.; et al. Regulation methods for the Zn/electrolyte interphase and the effectiveness evaluation in aqueous Zn-ion batteries. *Energy Environ. Sci.* **2021**, *14*, 5669–5689.
- (40) Zhang, S.; et al. Dual-Function Electrolyte Additive for Highly Reversible Zn Anode. *Adv. Energy Mater.* **2021**, *11*, 2102010.
- (41) Zhang, P.; Wu, Z.; Zhang, S.; Liu, L.; Tian, Y.; et al. Tannin acid induced anticorrosive film toward stable Zn-ion batteries. *Nano Energy* **2022**, *102*, 107721.
- (42) Chao, D.; et al. Toward High-Voltage Aqueous Batteries: Super- or Low-Concentrated Electrolyte? *Joule* **2020**, *4*, 1846–1851.
- (43) Peper, J. L.; Mayer, J. M. Manifesto on the Thermochemistry of Nanoscale Redox Reactions for Energy Conversion. *ACS Energy Lett.* **2019**, *4*, 866–872.
- (44) Boettcher, S. W.; Oener, S. Z.; Lonergan, M. C.; Surendranath, Y.; Ardo, S.; Brozek, C.; Kempler, P. A. Potentially Confusing: Potentials in Electrochemistry. *ACS Energy Lett.* **2021**, *6*, 261–266.
- (45) Yuan, Y.; et al. A Proton-Barrier Separator Induced via Hofmeister Effect for High-Performance Electrolytic MnO₂–Zn Batteries. *Adv. Energy Mater.* **2022**, *12*, 2103705.
- (46) Chuai, M.; et al. Theory-Driven Design of a Cationic Accelerator for High-Performance Electrolytic MnO₂–Zn Batteries. *Adv. Mater.* **2022**, *34*, 2203249.
- (47) Pei, A.; Zheng, G.; Shi, F.; Li, Y.; Cui, Y. Nanoscale Nucleation and Growth of Electrodeposited Lithium Metal. *Nano Lett.* **2017**, *17*, 1132–1139.
- (48) WINAND, R. ElectrocrySTALLIZATION: fundamental considerations and application to high current density continuous steel sheet plating *. *J. Appl. Electrochem.* **1991**, *21*, 377–385.
- (49) Ueda, M.; et al. Double-pulse technique as an electrochemical tool for controlling the preparation of metallic nanoparticles. *Electrochim. Acta* **2002**, *48*, 377–386.
- (50) Ely, D. R.; García, R. E. Heterogeneous Nucleation and Growth of Lithium Electrodeposits on Negative Electrodes. *J. Electrochem. Soc.* **2013**, *160*, A662.
- (51) Makkonen, L. Young's equation revisited. *J. Phys.: Condens. Matter* **2016**, *28*, 135001.
- (52) Kwok, D. Y.; Li, D.; Neumann, A. W. Fowkes' surface tension component approach revisited. *Colloid Surfaces A Physicochem. Eng. Asp.* **1994**, *89*, 181–191.
- (53) Hao, J.; et al. Designing Dendrite-Free Zinc Anodes for Advanced Aqueous Zinc Batteries. *Adv. Funct. Mater.* **2020**, *30*, 2001263.

□ Recommended by ACS

Addition of Dioxane in Electrolyte Promotes (002)-Textured Zinc Growth and Suppressed Side Reactions in Zinc-Ion Batteries

Tingting Wei, Guozhong Cao, et al.

FEBRUARY 08, 2023

ACS NANO

READ ▾

Prefabrication of “Trinity” Functional Binary Layers on a Silicon Surface to Develop High-Performance Lithium-Ion Batteries

Weibo Huang, Honghe Zheng, et al.

JANUARY 25, 2023

ACS NANO

READ ▾

Sustained-Compensated Interfacial Zincophilic Sites to Assist High-Capacity Aqueous Zn Metal Batteries

Xu Zeng, Tao Qian, et al.

FEBRUARY 13, 2023

NANO LETTERS

READ ▾

A Double-Functional Additive Containing Nucleophilic Groups for High-Performance Zn-Ion Batteries

Jiandong Wan, Zaiping Guo, et al.

JANUARY 03, 2023

ACS NANO

READ ▾

Get More Suggestions >